Quantum-confinement effects in InAs–InP core–shell nanowires

2007 J. Phys.: Condens. Matter 19 295219

(http://iopscience.iop.org/0953-8984/19/29/295219)

IOP PUBLISHING JOURNAL OF PHYSICS: CONDENSED MATTER

J. Phys.: Condens. Matter **19** (2007) 295219 (8pp) doi:10.1088/0953-8984/19/29/295219

Quantum-confinement effects in InAs–InP core–shell nanowires

Z Zanolli, M-E Pistol, L E Fröberg and L Samuelson

Solid State Physics/The Nanometer Structure Consortium, Lund University, Box 118, S-221 00 Lund, Sweden

E-mail: zanolli@pcpm.ucl.ac.be

Received 17 April 2007
Published 11 June 2007
Online at stacks.iop.org/JPhysCM/19/295219

Abstract

We report the detection of quantum confinement in single InAs–InP core–shell nanowires. The wires, having an InAs core with ∼25 nm diameter, are characterized by emission spectra in which two peaks are identified under high excitation intensity conditions. The peaks are caused by emission from the ground and excited quantized levels, due to quantum confinement in the plane perpendicular to the nanowire axis. We have identified different energy contributions in the emission spectra, related to the wurtzite structure of the wires, the strain between the wurtzite core and the shell, and the confinement energy of the InAs core. Calculations based on six-band strain-dependent $\mathbf{k}\cdot\mathbf{p}$ theory allow the theoretical estimation of the confined energy states in such materials, and we found these results to be in good agreement with those from the photoluminescence studies.

(Some figures in this article are in colour only in the electronic version)

1. Introduction

The investigation of the properties of nanometre-size materials is an essential step towards a better understanding of the fundamental physics underlying their behaviour and hence towards further developments in nanotechnologies. Semiconductor nanowires (NWs) have the double feature of providing a tool for the study of the physical properties of low-dimensional systems and, at the same time, of providing the building blocks of electronic and photonic nanoscale devices [1]. Nanoscale field-effect transistors [2–6], inverters [5, 6], and logic gates [6] are some examples of NW-based devices. One-dimensional (1D) electronics can also take advantage of the growth of heterostructures along the NW axis, as has been demonstrated in resonant tunnelling diodes [7] and single-electron transistors [8]. Concerning photonic applications, devices such as light-emitting diodes (LEDs) [4], photodetectors [9], and lasers [10, 11] based on NWs have been reported. The results achieved so far are encouraging

for pursuing developments in the bottom-up fabrication approach and, at the same time, for calling for investigations of the electrical and optical properties of NWs to define the conditions for future applications.

The NW structure is a favourable environment to achieve 1D systems, i.e. to force the motion of the electrons along only one direction, the NW axis. Indeed, if the NW diameter is small enough, the electrons will be confined by a potential well in the radial direction with a consequent energy quantization in that plane. Hence NWs exhibit physical properties which are intrinsically different from those of quantum dots and bulk materials. The Bohr radius of the exciton in a bulk crystal [12, 13] provides the length scale for the onset of quantum-confinement effects. This implies that in the nanowires presented here quantum confinement can be observed when the core diameter is smaller than 35 nm, the exciton Bohr radius in bulk InAs. When this condition is met, we expect the formation of quantized levels in both conduction and valence bands of the semiconductor. Analogously to what happens in a quantum well, the bandgap in a quantum wire is larger than the gap of the bulk material. Moreover, transitions between the localized quantum levels now become possible.

Electron quantum confinement was demonstrated via photoluminescence (PL) measurements in GaAs [14] and InP [15, 16] nanowires as a blue-shift of the emission energy with decreasing diameter of the wires, and via scanning tunnelling microscopy (STM) in Si nanowires [17]. In InAs nanowires with diameter smaller than 30 nm the observed drop in the wire conductance was explained as an effect of the quantum confinement [18]. We report here studies of quantum-confinement effects in InAs-based NWs. The wires were grown via chemical beam epitaxy (CBE) and the optical characterization was performed via low-temperature micro-photoluminescence measurements (μ-PL) on single NWs. Due to the low emission efficiency of uncapped InAs NWs, we chose to study InAs–InP core–shell structures similar to those reported in [19]. The shell material provides a passivation of the core surface, hindering the non-radiative electron–hole recombination through surface states, a mechanism that limits the emission efficiency of the core.

After taking into account the shift towards higher energies due to the strain and to the wurtzite structure of the InAs NWs, we have found that the PL peaks are further blue-shifted with respect to the bulk energy gap of the zinc-blende phase due to quantum confinement. Besides that, as a clear signature of level quantization, we report the observation of the first excited state above the gap. We compare the experimental results to accurate calculations based on six-band strain-dependent $\mathbf{k}\cdot\mathbf{p}$ theory in the so-called envelope function approximation [20] and we find good agreement between experiments and theory.

2. Methods of investigation

2.1. Sample fabrication

The nanowires are grown using CBE, which is a high-vacuum growth technique similar to molecular beam epitaxy, but using organometallic source molecules. The material is supplied in a beam directed towards the sample [21, 22] and—due to the low pressure—the mean free path of the material is much longer than the chamber size. The first step of the sample fabrication is the deposition of Au aerosol particles on an InAs(111)B substrate. The aerosol particles are produced in a home-built system [23], in which Au is evaporated, condensed and size selected. The size selection is important since it determines the diameter of the nanowire. In this study we used Au particles 20 nm and 40 nm wide, leading to ∼25 nm and ∼45 nm core diameters, respectively. The Au particles enhance the growth rate beneath them, resulting in rod-like structures on the surface with the Au particle sitting on top, schematically shown in figure 1(a).

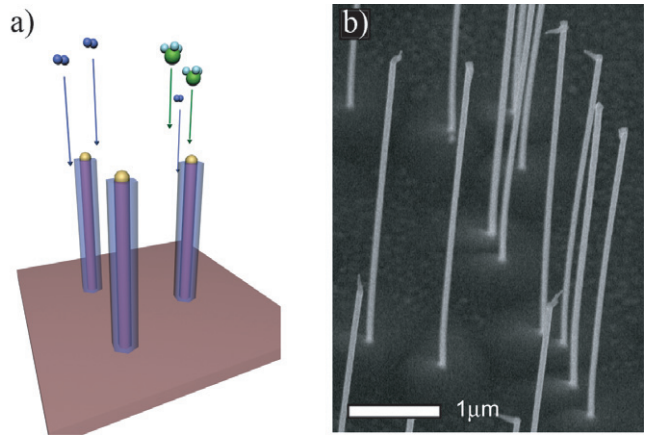

Figure 1. (a) Schematic representation of the growth process of InAs–InP core–shell NWs and (b) SEM image of the as-grown wires (25 nm core diameter, 20 nm shell thickness).

The most referenced growth model for nanowires is based on the vapour–liquid–solid (VLS) mechanism [24], in which material is supplied in the vapour phase which preferably condenses on the liquid metal–semiconductor alloy. This creates a stronger driving force for growth at the liquid–solid interface compared to the vapour–solid interface, and growth material precipitates out into the crystal from the alloy. However, since the growth temperature is lower than any melting point in the phase diagram, the nanowires in our system grow from a solid particle. This has led to the suggestion of vapour–solid–solid (VSS) growth [25, 26].

We have grown InAs wires at 425 °C, under conditions resulting in a wurtzite crystal structure of the core, and then lowered the temperature to 370 °C and switched precursors to allow for radial (20 nm thick) InP growth as in [19]. A scanning electron microscope (SEM) image of such a sample at an angle of 30° can be seen in figure 1(b). The sources used are tertiarybutylarsine (TBAs), tertiarybutylphosphine (TBP) and trimethylindium (TMIn) for As, P and In, respectively, and the corresponding pressures in the gas lines to the growth chamber are 1.5, 3.0 and 0.15 mbar. The TBAs and TBP are thermally cracked upon entering the growth chamber, while the TMIn decomposes on the substrate surface. During the shell growth, the axial nanowire growth is not fully suppressed, and InP grows under the Au particle under non-ideal conditions, as can be seen in figure 1(b) as an extra feature at the top of the wires.

2.2. PL measurements on single NWs

After growth, the NWs were mechanically transferred onto a gold patterned Si/SiO_2 substrate where single wires could be located and their optical properties studied at a single NW level. The substrate with the wires was inspected using an optical microscope (100 × objective, dark field) and—after PL measurements—an SEM to identify single wires that are more suitable for optical characterization, i.e. those wires which are well isolated and far from any other particle eventually present on the substrate by more than ∼20 μm. The spectra from single NWs were obtained using a μ-PL setup optimized for detection of radiation in the near-IR (0.9–2.0 μm). The NWs were excited with the 532 nm line of a frequency-doubled Nd–YAG laser. The laser light was focused onto the sample, mounted on the cold finger of a continuous-flow helium cryostat for low-temperature (∼5 K) measurements. The light emitted from the NW was collected by a long working distance reflective objective (NA = 0.28) of a microscope

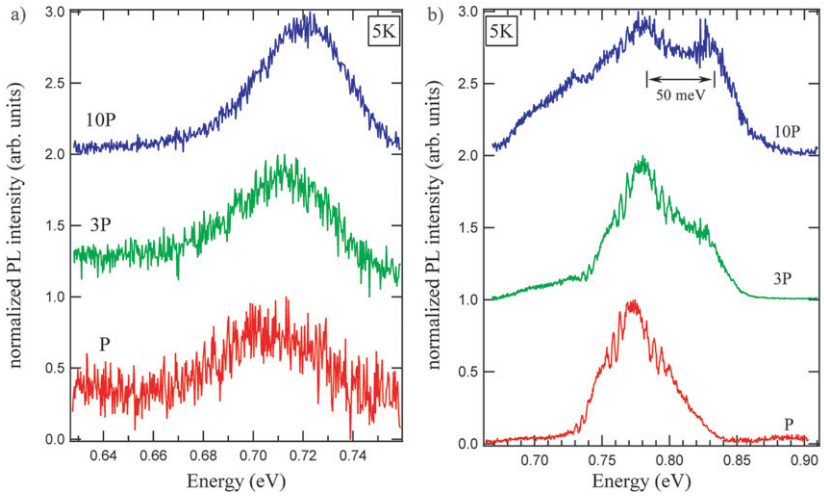

Figure 2. PL emission spectra at different excitation laser densities from 45 to 20 nm (a) and 25 to 20 nm (b) core–shell InAs–InP single NWs. In the 25 nm core wire the two peaks from the ground state and first excited quantized states are visible.

and was focused onto the entrance slit of a spectrometer. Then the emitted light was imaged or spectrally dispersed on the HgCdTe focal plane array of a liquid-N_2 cooled camera.

2.3. Calculations

For the interpretation of the experimental results, we initially computed the strain tensor profile of the NWs using linear continuum elasticity theory. Our calculation is fully three-dimensional and was done on a $100\times100\times100$ grid, where the strain energy was minimized by the conjugate gradient method. Using the so-obtained strain tensor element we computed the electronic states within the so-called $\mathbf{k}\cdot\mathbf{p}$ theory allowing mixing among six bands in the valence band [27]. The conduction band was treated in the single-band approximation. We included the piezoelectric polarization in the calculation. Since the structure is a wire we have a continuum of states, and it was necessary to compute a large number of eigenvalues in order to identify the radially excited states. The differential system was discretized on a grid and formulated as a finite difference problem. In order to get reasonable computing times we truncated the grid from $100\times100\times100$ to $60\times60\times60$ when doing the electronic structure calculation. In contrast to the power-law decay of the strain, the wavefunctions have an exponential decay in the barrier, and it is thus appropriate to use a smaller box for the electronic calculations than for the strain calculations. The Lanczos algorithm was used to fit the eigenvalues.

3. Results and discussion

To find evidence of quantum-confinement effects in InAs NWs we considered here two sets of NWs differing in their diameter, i.e. 25 and 45 nm in diameter. The PL spectra from such wires are shown in figures 2(a) and (b) for 45 nm and 25 nm core width, respectively. At low excitation power density, a single peak is detected at about 771 meV (FWHM = 50 meV) and 703 meV (FWHM = 60 meV), respectively. Evidence of state filling is visible in both spectra as an energy blue-shift of the main peak with the increase of the excitation power density [28]. The striking difference between the two samples is that in the emission from the 25 nm wire

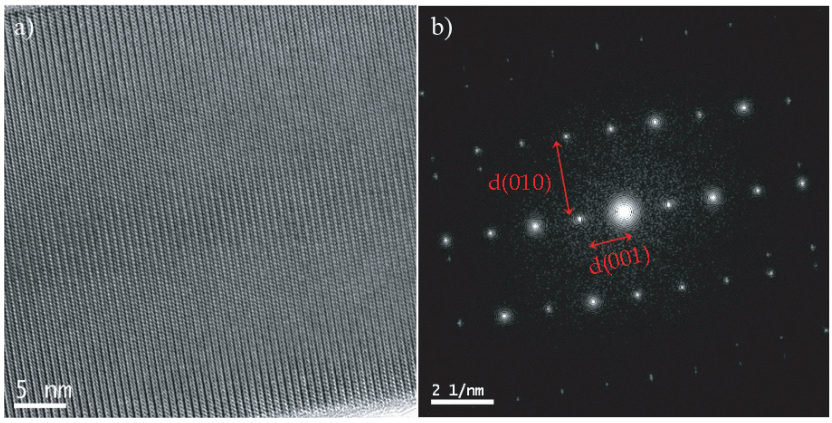

Figure 3. TEM image (a) and its Fourier transform (b) of an InAs wire (∼42 nm wide). The wurtzite lattice constants are $a_{wz} = 2\mathrm{d}(010)/\sqrt{3}$ and $c = \mathrm{d}(001)$. *(Courtesy of Jacob B Wagner.)*

at high excitation power density two peaks are visible at energies of about 781 and 831 meV. This can be interpreted as evidence of energy quantization in the radial direction, where the low-energy peak and the high-energy peak can be interpreted as the ground and first excited quantized levels, as we will discuss below.

In the analysis of these emission spectra one should consider the fact that there are different effects contributing to the blue-shift of the wire emission compared to bulk InAs zinc blende. First of all, the shell thicknesses of both NWs were 20 nm, so the energy shifts due to the strain are larger for the small core diameter wire, resulting in a higher emission energy.

We should also take into account the fact that these NWs have wurtzite (wz) crystal structure, while zinc blende (zb) is the crystal structure observed for bulk InAs and InP compounds. The wurtzite phase is demonstrated by the TEM analysis performed on such wires. Figure 3(a) shows the TEM image of a bare InAs NW together with the Fourier transform of the image, from which the lattice constants are measured as $a_{wz} = 4.2839$ Å and $c = 6.9954$ Å. This affects the energy gap of both materials, so the wz phases have a larger gap relative to the zb phases, as theoretical studies based on density functional theory (DFT) reveal [29, 30]. We should mention that the energy gap predicted via DFT is usually underestimated because it is an excited-state property and can be correctly described using many-body perturbation theory. This treatment is beyond the scope of this article, and the reader is referred to the work done by one of the authors on the calculation of the quasiparticle band structure in the so-called dynamically screened exchange approximation (GWA) [31, 32] of InAs in the wurtzite phase [33]. From this study it has been found that the difference in the energy gaps of wz and zb InAs is $\Delta\mathrm{gap} = 55.7$ meV, leading to 470.7 meV as the energy gap of InAs in the wurtzite phase at 0 K.

In the case of the InP compound, the energy gap of the wz phase has been measured in ∼50 nm thick nanowires to be ∼80 meV higher than the one of the corresponding zb phase [34]. Since the increase in energy gap due to the wz phase is higher in the InP than in the InAs material system, it follows[1] that the difference between the *a* lattice constant of the two materials in the wz phase is larger as compared to the zb case. Hence the lattice mismatch between the two materials is higher when they are in the wz phase and, consequently, the blue-

[1] In tight-binding approximation it can be shown that in direct band-gap III–V semiconductors a higher energy gap corresponds to a smaller *a* lattice constant.

Table 1. The confinement energies and the quantized energy levels for the InAs wires under study, with the inclusion of the strain effects due to the InP shell in zinc-blende materials. The energies are reported in meV, and the diameters in nm.

Au diam	InAs diam	$E_{\mathrm{QC}}\mathrm{e}^-$	$E_{\mathrm{QC}}\mathrm{h}^+$	E_{QC}	$E_{0\mathrm{c}}$	$E_{0\mathrm{v}}$	$E_{1\mathrm{c}}$	$E_{1\mathrm{v}}$
20	25	54	14.7	68.7	37	−586	79	−605
40	45	14	10.7	24.7	−3	−582	16	−587

shift in energy due to strain will be higher when InAs and InP are in the wz phase. We denote by $\Delta\mathrm{strain} = E_{\mathrm{strain\ WZ}} - E_{\mathrm{strain\ ZB}}$ the increase in the InAs emission energy due to this effect. We can summarize all the mentioned contributions to the InAs emission as follows:

$$E = E_{\mathrm{bulk\ WZ}} + E_{\mathrm{strain\ WZ}} + E_{\mathrm{QC}}, \tag{1}$$

where E is the measured emission energy, $E_{\mathrm{bulk\ WZ}}$ is the band gap of the bulk InAs in the wz phase and E_{QC} is the contribution given by quantum confinement.

From the data and the modelling reported in [19] it is possible to evaluate the difference in the confinement energy between the 25 and 45 nm core wires, $\Delta E_{\mathrm{QC}} = E_{\mathrm{QC}}(25\ \mathrm{nm}) - E_{\mathrm{QC}}(45\ \mathrm{nm})$. Indeed, for each diameter, the dependence of the measured emission energy E and that one calculated using eight-band strain-dependent $\mathbf{k}\cdot\mathbf{p}$ theory without the inclusion of quantum-confinement effects for the zb phase ($E_{\mathrm{calc}} = E_{\mathrm{bulk\ ZB}} + E_{\mathrm{strain\ ZB}}$) can be written as

$$E - E_{\mathrm{calc}} = \Delta\mathrm{strain} + \Delta\mathrm{gap} + E_{\mathrm{QC}}, \tag{2}$$

where we use the measured emission energies at low excitation power (771 and 703 meV) and the values obtained from an exponential fit of the calculated data, i.e. 567 and 537 meV for the 25–20 nm and 45–20 nm core–shell wires, respectively. Writing equation (2) for both (25 and 45 nm) core diameters and taking their difference leads to $\Delta E_{\mathrm{QC}} = 38$ meV. It is worth noting that this value is obtained without any assumption on Δstrain and Δgap.

Calculations of the confinement energies and of the energies of the ground ($E_{0\mathrm{c}}$, $E_{0\mathrm{v}}$) and first ($E_{1\mathrm{c}}$, $E_{1\mathrm{v}}$) excited states in InAs for both electrons and holes in the InAs/InP wire system were performed according to the method outlined in section 2.3. These calculations, whose results are summarized in table 1 and are visualized in figure 4, were done for wires having InAs cores 25 and 45 nm wide, which is the expected average diameter when the seed Au particle is 20 nm and 40 nm, respectively. The so-obtained confinement energy of both electrons and holes leads to $E_{\mathrm{QC}}(45\ \mathrm{nm}) = 24.7$ meV and $E_{\mathrm{QC}}(25\ \mathrm{nm}) = 68.7$ meV; hence $\Delta E_{\mathrm{QC\ calc}} = 44$ meV. Considering the uncertainties in the determination of the actual core diameter, we find that the results agree.

We then compared the calculated transition energies with the measured ones in the 25 nm wires at high excitation power density. The ground and first excited state emission energies are calculated as $E_0 = E_{0\mathrm{c}} - E_{0\mathrm{v}} = 623$ meV and $E_1 = E_{1\mathrm{c}} - E_{1\mathrm{v}} = 684$ meV, respectively. These values have to be compared with the first and second peaks in the measured spectrum at 781 and 831 meV. At first we notice that the energy difference between these peaks is about 50 meV and the calculated one is 61 meV. Hence the energy separation of the two peaks is reproduced well (within ∼10 meV) by our theoretical model. Moreover, since the calculations are performed for zb InAs and InP materials, the difference between the calculated and measured (at low excitation power density) values is given by $\Delta\mathrm{gap} + \Delta\mathrm{strain}$, which therefore amounts to

$$\Delta\mathrm{gap} + \Delta\mathrm{strain} = 148\ \mathrm{meV}. \tag{3}$$

If we then use the GW value for the difference in energy gaps ($\Delta\mathrm{gap} = 55.7$ meV), we obtain $\Delta\mathrm{strain} = 92.3$ meV.

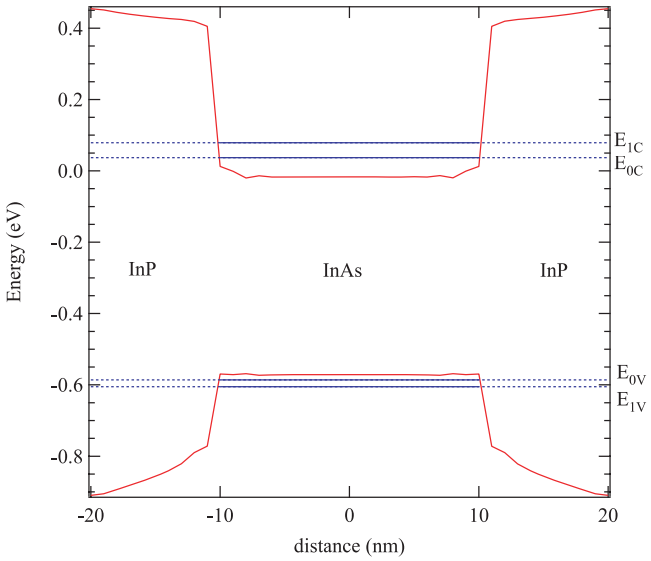

Figure 4. Location of the quantized energy levels with respect to the band structure. The discrete states are calculated for an InAs–InP 25–20 nm core–shell wire.

4. Conclusion

In this paper we have reported an optical study and modelling of quantum-confinement effects in the emission from the InAs core of InAs/InP core–shell strained nanowires. The PL measurements performed on single NWs having small (∼25 nm) core diameter are characterized by a double-peak emission due to the formation of quantized energy levels in the band structure. The energy separation between the fundamental and excited peak of about 50 meV is well reproduced by the theoretical calculations. Since the wires have the wurtzite crystal structure, while the calculations describe zinc-blende material systems, we have taken into account the increase in the actual energy gap and the difference in the strain between the wurtzite materials. Each of these two effects causes a blue-shift of the InAs emission to a total contribution of 148 meV. Beside this increase in emission energy, the observed fundamental peak is further shifted due to quantum confinement, consistently with the calculations. Finally, we compared the experimental and calculated energy difference between the confinement energy in 25 and 45 nm wires, finding that the two estimations are in agreement.

Acknowledgments

This research was conducted within the Nanometre Structure Consortium in Lund and supported by the European Community's Human Potential Program under contract HPRN-CT-2002-00298, the EU program NODE 015783, the Swedish Foundation for Strategic Research (SSF), the Swedish Research Council (VR) and the Knut and Alice Wallenberg Foundation. Dr J B Wagner is gratefully acknowledged for TEM imaging.

References

[1] Hu J, Odom T W and Lieber C M 1999 *Acc. Chem. Res.* **32** 435–5
[2] Bryllert T, Wernersson L-E, Fröberg L and Samuelson L 2006 *IEEE-Electron Device Lett.* **27** 323–5

[3] Bryllert T, Wernersson L-E, Löwgren T and Samuelson L 2006 *Nanotechnology* **17** S227–30
[4] Duan X F, Huang Y, Cui Y, Wang J and Lieber C M 2001 *Nature* **409** 66–9
[5] Cui Y and Lieber C M 2001 *Science* **291** 851–3
[6] Huang Y, Duan X F, Cui Y, Lauhon L J, Kim K-H and Lieber C M 2001 *Science* **291** 630–3
[7] Björk M T, Ohlsson B J, Thelander C, Persson A, Deppert K, Wallenberg L R and Samuelson L 2002 *Appl. Phys. Lett.* **81** 4458–60
[8] Thelander C, Mårtensson T, Ohlsson B J, Larsson M W, Wallenberg L R and Samuelson L 2003 *Appl. Phys. Lett.* **83** 2052–4
[9] Wang J, Gudiksen M S, Duan X, Cui Y and Lieber C M 2001 *Science* **293** 1455–7
[10] Huang M H, Mao S, Feick H, Yan H, Wu Y, Kind H, Weber E, Russo R and Yang P 2001 *Science* **292** 1897–9
[11] Johnson J C, Yan H Q, Schaller R D, Haber L H, Saykally R J and Yang P D 2001 *J. Phys. Chem.* B **105** 11387–90
[12] Yoffe A D 1993 *Adv. Phys.* **42** 173–266
[13] Ashcroft N W and Mermin N D 1976 *Solid State Physics* (Fortworth, TX: Harcourt Brace College Publishers) pp 626–8
[14] Duan X *et al* 2000 *Appl. Phys. Lett.* **76** 1116–8
[15] Gudiksen M S, Wang J and Lieber C M 2002 *J. Phys. Chem.* B **106** 4036–9
[16] Bhunia S, Kawamura T, Watanabe Y, Fujikawa S and Tokushima K 2003 *Appl. Phys. Lett.* **83** 3371–3
[17] Ma D D D, Lee C S, Au F C K, Tong S Y and Lee S T 2003 *Science* **299** 1874–7
[18] Thelander C, Björk M T, Larsson M W, Hansen A E, Wallenberg L R and Samuelson L 2004 *Solid State Commun.* **131** 573–9
[19] Zanolli Z, Fröberg L E, Björk M T, Pistol M-E and Samuelson L 2007 Fabrication, optical characterization and modeling of strained core–shell nanowires *Thin Solid Films* **515** 793–6
[20] Gershoni D, Henry C H and Baraff G A 1993 *IEEE J. Quantum Electron.* **29** 2433–50
[21] Ohlsson B J, Björk M T, Magnusson M H, Deppert K, Samuelson L and Wallenberg L R 2001 *Appl. Phys. Lett.* **79** 3335–7
[22] Jensen L E, Björk M T, Jeppesen S, Persson A I, Ohlsson B J and Samuelson L 2004 *Nano Lett.* **4** 1961–4
[23] Magnusson M H, Deppert K, Malm J-O, Bovin J-O and Samuelson L 1999 *J. Nanoparticle Res.* **2** 243–51
[24] Wagner R S and Ellis W C 1964 *Appl. Phys. Lett.* **4** 89–90
[25] Persson A I, Larsson M W, Stenström S, Ohlsson B L, Samuelson L and Wallenberg L R 2004 *Nat. Mater.* **3** 677–81
[26] Dick K A, Deppert K, Mårtensson T, Mandl B, Samuelson L and Seifert W 2005 *Nano Lett.* **5** 761–4
[27] Pryor C 1998 *Phys. Rev.* B **57** 7190–5
[28] Castrillo P, Hessmann D, Pistol M-E, Anand S, Carlsson N, Seifert W and Samuelson L 1995 *Appl. Phys. Lett.* **67** 1905–7
[29] Yeh C-Y, Wei S-H and Zunger A 1994 *Phys. Rev.* B **50** 2715–8
[30] Murayama M and Nakayama T 1994 *Phys. Rev.* B **49** 4710–24
[31] Hedin L 1965 *Phys. Rev.* **139** A796–823
[32] Hedin L and Lundqvist S 1969 *Solid State Physics* vol 23, ed F Seitz, D Turnbull and H Ehrenreich (New York: Academic) p 1
[33] Zanolli Z, Furthmüller J, Fuchs F, von Barth U and Bechstedt F 2007 GW band structure of InAs and GaAs in the wurtzite phase *Phys. Rev.* B at press
[34] Mattila M, Hakkarainen T, Mulot M and Lipsanen H 2006 *Nanotechnology* **17** 1580–3